

1 **STARRPeaker: Uniform processing and accurate identification of STARR-seq active**
2 **regions**

3

4 Donghoon Lee¹, Manman Shi², Jennifer Moran², Martha Wall², Jing Zhang^{1,3}, Jason Liu³,
5 Dominic Fitzgerald², Yasuhiro Kyono², Lijia Ma^{2,4}, Kevin P White^{2,5*}, Mark Gerstein^{1,3,6,7*}

6

7 1 Program in Computational Biology and Bioinformatics, Yale University, New Haven, CT
8 06520, USA

9 2 Institute for Genomics and System Biology, University of Chicago, Chicago, IL, 60637, USA

10 3 Department of Molecular Biophysics and Biochemistry, Yale University, New Haven, CT
11 06520, USA

12 4 School of Life Sciences, Westlake University, Hangzhou, 310024, China

13 5 Tempus Labs, Inc. Chicago IL 60654, USA

14 6 Department of Computer Science, Yale University, New Haven, CT 06520, USA

15 7 Department of Statistics and Data Science, Yale University, New Haven, CT 06520, USA

16

17 * Corresponding author

18 E-mail: pi@gersteinlab.org

19

20

21 **Abstract**

22 High-throughput reporter assays, such as self-transcribing active regulatory region sequencing
23 (STARR-seq), allow for unbiased and quantitative assessment of enhancers at a genome-wide
24 level. Recent advances in STARR-seq technology have employed progressively more complex
25 genomic libraries and increased sequencing depths, to assay larger sized regions, up to the entire
26 human genome. These advances necessitate a reliable processing pipeline and peak-calling
27 algorithm. Most STARR-seq studies have relied on chromatin immunoprecipitation sequencing
28 (ChIP-seq) processing pipeline to identify peaks. However, there are key differences in STARR-
29 seq versus ChIP-seq data: STARR-seq uses transcribed RNA to measure enhancer activity,
30 making determining the basal transcription rate important. Furthermore, STARR-seq coverage is
31 non-uniform, overdispersed, and often confounded by sequencing biases such as GC content and
32 mappability. Moreover, here, we observed a clear correlation between RNA thermodynamic
33 stability and STARR-seq readout, suggesting that STARR-seq might be sensitive to RNA
34 secondary structure and stability. Considering these findings, we developed STARRPeaker: a
35 negative binomial regression framework for uniformly processing STARR-seq data. We applied
36 STARRPeaker to two whole human genome STARR-seq experiments; HepG2 and K562. Our
37 method identifies highly reproducible and epigenetically active enhancers across replicates.
38 Moreover, STARRPeaker outperforms other peak callers in terms of identifying known
39 enhancers. Thus, our framework optimized for processing STARR-seq data accurately
40 characterizes cell-type-specific enhancers, while addressing potential confounders.

41

42 **Keywords:** STARR-seq, peak caller, enhancer, non-coding

43

44 **Introduction**

45 The transcription of eukaryotic genes is precisely coordinated by an interplay between cis-
46 regulatory elements. For example, enhancers and promoters serve as platforms for transcription
47 factors (TF) to bind and interact with each other, and their interactions are often required to
48 initiate transcription^{1,2}. Enhancers, which are often located distantly from the transcribed gene
49 body itself, play critical roles in the upregulation of gene transcription. Enhancers are cell-type
50 specific and can be epigenetically activated or silenced to modulate transcriptional dynamics
51 over the course of development. Enhancers can be found upstream or downstream of genes, or
52 even within introns³⁻⁵. They function independent from their orientation, do not necessarily
53 regulate the closest genes, and sometimes regulate multiple genes at once^{6,7}. In addition, several
54 recent studies have demonstrated that some promoters – termed E-promoters – may act as
55 enhancers of distal genes^{8,9}.

56
57 Unlike protein-coding genes, enhancers do not yet have a well-characterized consensus sequence.
58 Therefore, identifying enhancers in an unbiased fashion is challenging. The non-coding territory
59 occupies over 98% of the genome landscape, making the search space very broad. Moreover, the
60 activity of enhancers depends on the physiological condition and epigenetic landscape of the
61 cellular environment, complicating the fair assessment of enhancer function.

62
63 Previously, putative regulatory elements were computationally predicted, indirectly, by profiling
64 DNA accessibility (using DNase-seq, FAIRE-seq, and ATAC-seq) as well as histone
65 modifications (ChIP-seq) that are linked to regulatory functions¹⁰⁻¹². More recently, researchers
66 have developed high-throughput episomal (exogenous) reporter assays to directly measure

67 enhancer activity across the whole genome, specifically massively parallel reporter assays
68 (MPRA)^{13,14} and self-transcribing active regulatory region sequencing (STARR-seq)^{15,16}. These
69 assays allow for quantitative assessment of enhancer activity in a high-throughput fashion.

70

71 In STARR-seq, candidate DNA fragments are cloned downstream of a reporter gene into the 3'
72 untranslated region (UTR). After transfecting the plasmid pool into host cells, one can measure
73 the regulatory potential by high-throughput sequencing of the 3' UTR of the expressed reporter
74 gene mRNA. These exogenous reporters enable accurate and unbiased assessment of enhancer
75 activity at the whole genome level, independent of chromatin context. Unlike MPRA – which
76 utilizes barcodes – STARR-seq produces self-transcribed RNA fragments that can be directly
77 mapped onto the genome. The activities of enhancers are measured by comparing the amount of
78 RNA produced from the input DNA library. STARR-seq has several technical advantages over
79 MPRA. Library construction is relatively simple because barcodes are not needed. In addition,
80 candidate enhancers are cloned instead of synthesized, allowing the assay to test extended
81 sequence contexts (>500 bp) for enhancer activity, which studies have shown to be critical for
82 functional activity¹⁷. Importantly, STARR-seq can be scaled to the whole genome level for
83 unbiased scanning for functional elements. However, scaling STARR-seq to the human genome
84 is still very challenging, primarily due to its massive size. A more complex genomic DNA
85 library, a higher sequencing depth, and increased transfection efficiency are required to cover the
86 whole human genome¹⁶, which could ultimately introduce biases.

87

88 Processing of STARR-seq is somewhat similar to chromatin immunoprecipitation sequencing
89 (ChIP-seq), where protein-crosslinked DNA is immunoprecipitated and sequenced. A typical

90 ChIP-seq processing pipeline identifies genomic regions over-represented by sequencing tags in
91 a ChIP sample compared to a control sample. STARR-seq data is compatible with most ChIP-
92 seq peak callers. Hence, previous studies on STARR-seq have largely relied on peak calling
93 software developed for ChIP-seq such as MACS2^{16,18,19}. However, one must be cautious using
94 ChIP-seq peak callers, at least without re-tuning default parameters optimized for processing
95 transcription factor ChIP-seq²⁰.

96

97 In this paper, we describe key differences in the processing of STARR-seq versus ChIP-seq data.
98 Due to increased complexity of the genomic screening library and sequencing depth
99 requirements, STARR-seq coverage is highly non-uniform. This leads to a lower signal-to-noise
100 ratio than a typical ChIP-seq experiment and makes estimating the background model more
101 challenging, which could ultimately lead to false positives peaks. In addition, STARR-seq
102 measures more of a continuous activity similar to quantification in RNA-seq than a discrete
103 binding event. Therefore, STARR-seq peaks should be further evaluated using a notion of
104 activity score. These differences necessitate a unique approach to processing STARR-seq data.

105

106 We propose an algorithm optimized for processing and identifying functionally active enhancers
107 from STARR-seq data, which we call STARRPeaker. This approach statistically models the
108 basal level of transcription, accounting for potential confounding factors, and accurately
109 identifies reproducible enhancers. We applied our method to two whole human STARR-seq
110 datasets and evaluated its performance against previous methods. We also compared an R
111 package, BasicSTARRseq, developed to process peaks from the first STARR-seq data¹⁵, which
112 models enrichment using a binomial distribution. We benchmarked our peak calls against known

113 human enhancers. Thus, our findings support that STARRPeaker will be a useful tool for
114 uniformly processing STARR-seq data.

115

116 **Materials and Methods**

117

118 *Precise measurement of STARR-seq coverage*

119 We binned the genome using a sliding window of length, l , and step size, s . Based on the average
120 size of the STARR-seq library, we defined a 500 bp window length with a 100 bp step size to be
121 the default parameter. Based on generated genomic bins, we calculated the coverage of both
122 STARR-seq input and output mapped to each bin. For calculating the sequence coverage, other
123 peak callers and many visualization tools commonly use the start position of the read^{15,21,22}.
124 However, given that the average sizes of the fragments inserted in STARR-seq libraries were
125 approximately 500 bp, we expected that the read coverage using the start position of read may
126 shift the estimate of the summit of signal and dilute the enrichment. Some peak callers have used
127 read densities of forward and reverse strand separately to overcome this issue^{23,24}. To precisely
128 measure the coverage of STARR-seq input and output, we first inferred the size of the fragment
129 insert from paired-end reads and used the center of the fragment insert, instead of start position
130 of the read, to calculate coverage. For inferring the size of fragment insert, we first strictly
131 filtered out reads that were not properly paired and chimeric. Chimeric alignments are reads that
132 cannot be linearly aligned to a reference genome, implying a potential discrepancy between the
133 sequenced genome and the reference genome and indicative of structural variation²⁵. We also
134 filtered out read pairs that had a fragment insert size less than l_{max} and greater than l_{min} . By
135 default, we filtered out fragment insert sizes less than 100 bp and greater than 1,000 bp. After

136 filtering out spurious read-pairs, we estimated the center of the fragment insert and counted the
137 fragment depth for each genomic bin. We compared the coverage calculated using the start of
138 read against the center of fragment insert and observed both a shift in the location of enrichment
139 summit and a difference in enrichment level (**Figure 1**).

140

141 *Controlling for potential systemic bias in sequencing and STARR-seq library preparation*

142 STARR-seq measures the ratio of transcribed RNA to DNA for a given test region and
143 determines whether the test region can facilitate transcription at a higher rate than the basal level.
144 This is based on the assumption that the basal transcriptional level stays relatively constant
145 across the genome and the transcriptional rate is a reflection of the regulatory activity of a test
146 region. However, this may not always be true, and one needs to consider potential systemic
147 biases when analyzing the result. Unlike ChIP-seq where both the experiment and input controls
148 are from the same DNA origin, STARR-seq experiments measure the regulatory potential from
149 the abundance of transcribed RNA, which adds a layer of complexity. For example, RNA
150 structure and co-transcriptional folding might potentially influence the readout of STARR-seq
151 experiments²⁶. Single-stranded RNA starts to fold upon transcription and the resulting RNA
152 structure might influence the measurement of regulatory activity. Previously, researchers
153 suggested a potential linkage between RNA secondary structure and transcriptional regulation²⁷.
154 In addition, the resulting transcribed RNA undergoes a series of post-transcriptional regulation,
155 and RNA stability might play a critical role. Moreover, previous reports have shown that the
156 degradation rates vary significantly across the genome and RNA degradation rates are the main
157 determinant of cellular RNA levels²⁸. Furthermore, RNA stability correlates with
158 functionality^{29,30}.

159

160 There are also intrinsic sequencing biases in library preparation. A genome-wide reporter library
161 is made from randomly sheared genomic DNA, but DNA fragmentation is often non-random³¹.
162 Studies have also suggested that epigenetic mechanisms and CpG methylation may influence
163 fragmentation³². Furthermore, the isolated polyadenylated RNAs are reverse transcribed and
164 PCR is amplified before sequenced, and this process can further confound the sequenced
165 candidate fragments.

166

167 To unbiasedly test for the regulatory activity, a model needs to control for these potential
168 systemic biases inherent to generating STARR-seq data. As we expected, we observed that
169 STARR-seq coverage for both input and output are confounded by potential sequencing bias
170 (**Figure 2**). Notably, STARR-seq coverage significantly correlated with GC content (PCC 0.61;
171 P-val 1E-299), mappability (PCC 0.45; P-val 2.9E-148), and RNA thermodynamic stability
172 (PCC -0.55; P-val 0). Hence, to unbiasedly identify the activity peaks from STARR-seq, we
173 developed a model that accounts for variability of tested candidate fragments.

174

175 *Accurate modelling of STARR-seq coverage using negative binomial regression*

176 To model the fragment coverage data from STARR-seq using discrete probability distribution,
177 we assumed that each genomic bin is independent and identically distributed, as specified in
178 Bernoulli trials³³. That is, each test fragment can only map to a single fixed-length bin. Therefore,
179 we only considered a non-overlapping subset of bins for modeling and fitting the distribution.
180 We also excluded bins not covered by any genomic input or normalized input coverage was less
181 than a minimum quantile t_{min} , since these regions do not have sufficient power to detect

182 enrichment. We simulated and fitted various discrete probability distributions to STARR-seq
183 coverage. We observed that the STARR-seq coverage data was overdispersed and fitted the best
184 with negative binomial distribution (**Figure 3A**). We also noticed a slight negative enrichment,
185 indicating that some candidate fragments can silence the basal transcriptional activity. A Q-Q
186 plot of simulated coverage further demonstrated that the negative binomial model provides the
187 best fit for the data (**Figure 3B**).

188

189 *Peak caller*

190 To accurately model the ratio of STARR-seq sequence coverage (RNA) to input sequence
191 coverage (DNA) while controlling for potential confounding factors, we applied a negative
192 binomial regression. The overview of our model is outlined in **Figure 4**. Our model starts by
193 fitting an analytical distribution to the observed fragment coverage across each genomic bin. In
194 doing so, we use covariates to model expected counts in the form of multiple regression. Once
195 regression coefficients are estimated from a set of data, we can evaluate the likelihood of
196 observing the fragment count for each bin and assign p-values. Ultimately, bins with significant
197 enrichments are selected based on an adjusted p-values threshold, and they are fine-tuned to the
198 summit of the peak fragment enrichment.

199

200 Let Y be a vector of STARR-seq output (RNA) coverage, then y_i for $1 \leq i \leq n$ denotes the
201 number of RNA fragments from STARR-seq experiment mapped to the i -th bin from the total of
202 n genomic bins. Let t_i be the number of input library (DNA) mapped to the i -th bin. We define
203 X be the matrix of covariates where \vec{x}_i is the vector of covariates corresponding to the i -th bin,
204 and x_{ij} is the j -th covariate for the i -th bin.

205

206 Negative binomial distribution

207 A negative binomial distribution, which arises from a Gamma-Poisson mixture, can be
208 parametrized as follows³⁴⁻³⁶ (see Supplementary Methods for derivation).

209

$$f_Y(y_i|\mu_i, \theta) = \frac{\Gamma(y_i + \theta)}{\Gamma(y_i + 1) \cdot \Gamma(\theta)} \cdot \left(\frac{\theta}{\theta + \mu_i}\right)^\theta \cdot \left(\frac{\mu_i}{\theta + \mu_i}\right)^{y_i}$$

210

211 A negative binomial is a generalization of a Poisson regression that allows the variance to be
212 different from the mean, shaped by the dispersion parameter θ . The variance for the NB2 model
213 is given as

214

$$\sigma^2 = \mu + \frac{\mu^2}{\theta}$$

215

216 We assume that the majority of genomic bins will have a basal level of transcription, and the
217 count of RNA fragments at each i -th bin follows the traditional negative binomial (NB2)
218 distribution. The expected fragment counts, $E(y_i)$, represents the mean incidence, μ_i .

219

$$y_i \sim NB(\mu_i, \theta)$$

$$E(y_i) = \mu_i$$

220

221 Negative binomial regression model

222 The regression term for the expected RNA fragment count can be expressed in terms of a linear
223 combination of explanatory variables, a set of m covariates (\vec{x}). We use the input library variable
224 t_i as one covariate. For simplicity, we denote t_i as x_{0i} hereafter.

225

$$\begin{aligned}\ln \mu_i &= \beta_0 x_{0i} + \beta_1 x_{1i} + \dots + \beta_m x_{mi} \\ \mu_i &= \exp(\beta_0 x_{0i} + \beta_1 x_{1i} + \dots + \beta_m x_{mi}) \\ \mu_i &= \exp(\vec{x}_i^T \beta)\end{aligned}$$

226

227 Alternatively, instead of using the input library variable t_i as one covariate, we can directly use it
228 as an offset variable. One advantage of using the input variable as an “exposure” to the RNA
229 output coverage is that it allows us to directly model the basal transcription rate (the ratio of
230 RNA to DNA) as a rate response variable. More details on this alternative parametrization are
231 described in the Supplementary Methods.

232

233 Maximum-likelihood estimation

234 We fit the model and estimate regression coefficients using the maximum likelihood method,
235 where log-likelihood function is shown as follows.

236

$$\mathcal{L}_{NB}(\mu|y, \theta) = \sum_{i=1}^n y_i \ln\left(\frac{\mu_i}{\theta + \mu_i}\right) + \theta \ln\left(\frac{\theta}{\theta + \mu_i}\right) + \ln\left(\frac{\Gamma(y_i + \theta)}{\Gamma(y_i + 1) \cdot \Gamma(\theta)}\right)$$

237

238 Substituting μ_i with the regression term, the log-likelihood function can be parametrized in terms
239 of regression coefficients, β .

240

$$\mathcal{L}_{NB}(\beta|y, \theta) = \sum_{i=1}^n y_i \ln\left(\frac{e^{\bar{x}_i \beta}}{\theta + e^{\bar{x}_i \beta}}\right) + \theta \ln\left(\frac{\theta}{\theta + e^{\bar{x}_i \beta}}\right) + \ln\left(\frac{\Gamma(y_i + \theta)}{\Gamma(y_i + 1) \cdot \Gamma(\theta)}\right)$$

241

242 We can determine the maximum likelihood estimates of the model parameters by setting the first
243 derivative of the log-likelihood with respect to β , the gradient, to zero, and there is no analytical
244 solution for $\hat{\beta}$. Numerically, we iteratively solve for the regression coefficients β and the
245 dispersion parameter θ , alternatively, until both parameters converge.

246

247 Estimation of P-value

248 Finally, we calculate a P-value based on the fitted value of the i -th bin from the cumulative
249 distribution function of negative binomial distribution, and we assign false discovery rate using
250 Benjamini & Hochberg method³⁷.

251

$$\begin{aligned} P\text{-value} &= \Pr(x \geq y_i) = 1 - CDF(x = y_i - 1) \\ &= 1 - \sum_{i=0}^{\hat{y}_i - 1} \binom{\hat{y}_i + \theta - 1}{\hat{y}_i} \frac{\theta}{\theta + \hat{y}_i} \left(1 - \frac{\theta}{\theta + \hat{y}_i}\right)^\theta \end{aligned}$$

252

253 **Source code and data availability**

254 We implemented the method described in this article as a Python software package called
255 STARRPeaker. The software package can be downloaded, installed, and readily used to call
256 peaks from any STARR-seq dataset. The STARRPeaker package, as well as source code and

257 documentation, is freely available at: <http://github.com/gersteinlab/starrpeaker>. Data used in the
258 analysis will be made available from the Gene Expression Omnibus for public use.
259 DNase-seq and ChIP-seq data used for the analysis is publicly available from the ENCODE
260 portal (<https://www.encodeproject.org/>). The specific accession codes used for the analysis are
261 listed in Supplementary Table S3. GC content was downloaded from the UCSC Genome
262 Browser (<http://hgdownload.cse.ucsc.edu/gbdb/hg38/bbi/gc5BaseBw/>), and the mappability
263 track was created using gem-library software³⁸ with a k-mer size of 100 bp and the reference
264 human genome build hg38.

265

266 **Results**

267 We applied our peak calling algorithm to two whole human genome STARR-seq experiments,
268 K562 and HepG2, utilizing origin of replication-based (ORI) plasmids. Using this dataset, we
269 evaluated the quality and characteristics of identified enhancers as well as the performance of the
270 peak caller by comparing to external enhancer datasets.

271

272 ***Accurate identification of highly reproducible enhancers***

273 To evaluate the quality of enhancers identified from STARRPeaker, we uniformly called peaks
274 from the whole human genome STARR-seq dataset using methods previously used to identify
275 enhancers from STARR-seq data, namely BasicSTARRseq and MACS2, using recommended
276 settings. We first compared the level of epigenetic profile enrichment around the peaks. We
277 observed higher enrichment of DNase hypersensitive sites, as well as more distinct double-peak
278 patterns of H3K27ac and H3K4me1, using STARR-seq versus BasicSTARRseq or MACS2
279 (**Figure 5**). We also aggregated the transcription factor binding sites assayed by ChIP-seq around

280 peaks, and we observed significant enrichment of transcription factor binding events compared
281 to peaks identified by other methods. Furthermore, we compared STARRPeaker peaks and
282 others to previously characterized enhancers by CAGE³⁹, MPRA^{17,40}, and STARR-seq¹⁹ in
283 HepG2 or K562 cell line (**Figure 6**). We observed a higher fraction of STARRPeaker peaks
284 overlap with external datasets.

285

286 **Discussion**

287 We developed a statistically rigorous analysis pipeline for STARR-seq data in a software
288 package named STARRPeaker. STARRPeaker has several key improvements over previous
289 peak identification methods including (1) accurate quantification of STARR-seq coverage based
290 on inferred fragment size from paired-end reads; (2) use of a negative binomial distribution to
291 account for overdispersion in bin counts; and (3) modeling of STARR-seq coverage as a function
292 of input and potential confounding variables in STARR-seq signal. We applied our method to
293 two whole human genome ORI-STARR-seq datasets and demonstrated that it can unbiasedly
294 identify a set of STARR-seq-positive regions better than previous methods. The STARR-seq
295 peaks were enriched with epigenetic marks relevant to enhancers and overlapped better with
296 previously known enhancers than previous methods.

297

298 To completely understand how noncoding regulatory elements can modulate transcriptional
299 programs in human, STARR-seq active regions must be further characterized and validated
300 within the cellular context. Currently, CRISPR-based screens are limited to a small number of
301 selected targets. Our method can aid in prioritize candidate regions in unbiased fashion to
302 maximize the functional characterization efforts.

303

304 **Funding**

305 We acknowledge support from the NIH and from the AL Williams Professorship funds.

306

307 **Acknowledgements**

308 We thank Jinrui Xu and Joel Rozowsky for thoughtful discussion about CHIP-seq processing,

309 Michael Rutenberg Schoenberg and Zhen Chen for thoughtful discussion about RNA folding

310 biology, and all other members of the Gerstein and White laboratories for advice and critical

311 feedback on the manuscript.

312

313 **Author Contributions**

314 D.L., M.S., K.W., and M.G. conceived the project. D.L. and M.G. drafted the manuscript. D.L.

315 developed the STARRPeaker software package. M.S., J.M., M.W., D.F., Y.K., and L.M.

316 performed experimental work. M.W. performed experimental validation. D.L., J.Z., and J.L.

317 performed the downstream analysis. M.G. and K.W. provided funding and supervised the project.

318

319

320 **References**

- 321 1. Muerdter, F., Boryń, Ł. M. & Arnold, C. D. STARR-seq — Principles and applications.
322 *Genomics* **106**, 145–150 (2015).
- 323 2. Yáñez-Cuna, J. O., Kvon, E. Z. & Stark, A. Deciphering the transcriptional cis-regulatory
324 code. *Trends Genet.* **29**, 11–22 (2013).
- 325 3. Lettice, L. A. *et al.* A long-range Shh enhancer regulates expression in the developing
326 limb and fin and is associated with preaxial polydactyly. *Hum. Mol. Genet.* **12**, 1725–1735
327 (2003).
- 328 4. Banerji, J., Rusconi, S. & Schaffner, W. Expression of a beta-globin gene is enhanced by
329 remote SV40 DNA sequences. *Cell* **27**, 299–308 (1981).
- 330 5. Sagai, T., Hosoya, M., Mizushina, Y., Tamura, M. & Shiroishi, T. Elimination of a long-
331 range cis-regulatory module causes complete loss of limb-specific Shh expression and
332 truncation of the mouse limb. *Development* **132**, 797–803 (2005).
- 333 6. Melo, C. A. *et al.* eRNAs Are Required for p53-Dependent Enhancer Activity and Gene
334 Transcription. *Mol. Cell* **49**, 524–535 (2013).
- 335 7. Sanyal, A., Lajoie, B. R., Jain, G. & Dekker, J. The long-range interaction landscape of
336 gene promoters. *Nature* **489**, 109–13 (2012).
- 337 8. Dao, L. T. M. *et al.* Genome-wide characterization of mammalian promoters with distal
338 enhancer functions. *Nat. Genet.* **49**, 1073–1081 (2017).
- 339 9. Diao, Y. *et al.* A tiling-deletion-based genetic screen for cis-regulatory element
340 identification in mammalian cells. *Nat. Methods* **14**, 629–635 (2017).
- 341 10. Ernst, J. & Kellis, M. ChromHMM: automating chromatin-state discovery and
342 characterization. *Nat. Methods* **9**, 215–216 (2012).

- 343 11. Hoffman, M. M. *et al.* Unsupervised pattern discovery in human chromatin structure
344 through genomic segmentation. *Nat. Methods* **9**, 473–476 (2012).
- 345 12. Sethi, A. *et al.* A cross-organism framework for supervised enhancer prediction with
346 epigenetic pattern recognition and targeted validation. *bioRxiv* 385237 (2018).
347 doi:10.1101/385237
- 348 13. Patwardhan, R. P. *et al.* Massively parallel functional dissection of mammalian enhancers
349 in vivo. *Nat. Biotechnol.* **30**, 265–270 (2012).
- 350 14. Melnikov, A. *et al.* Systematic dissection and optimization of inducible enhancers in
351 human cells using a massively parallel reporter assay. *Nat. Biotechnol.* **30**, 271–277
352 (2012).
- 353 15. Arnold, C. D. *et al.* Genome-wide quantitative enhancer activity maps identified by
354 STARR-seq. *Science* **339**, 1074–7 (2013).
- 355 16. Liu, Y. *et al.* Functional assessment of human enhancer activities using whole-genome
356 STARR-sequencing. *Genome Biol.* **18**, 219 (2017).
- 357 17. Klein, J. C. *et al.* A systematic evaluation of the design, orientation, and sequence context
358 dependencies of massively parallel reporter assays. *bioRxiv* 576405 (2019).
359 doi:10.1101/576405
- 360 18. Johnson, G. D. *et al.* Human genome-wide measurement of drug-responsive regulatory
361 activity. *Nat. Commun.* **9**, 5317 (2018).
- 362 19. Rathert, P. *et al.* Transcriptional plasticity promotes primary and acquired resistance to
363 BET inhibition. *Nature* **525**, 543–547 (2015).
- 364 20. Koohy, H., Down, T. A., Spivakov, M. & Hubbard, T. A comparison of peak callers used
365 for DNase-Seq data. *PLoS One* **9**, e96303 (2014).

- 366 21. Uren, P. J. *et al.* Site identification in high-throughput RNA-protein interaction data.
367 *Bioinformatics* **28**, 3013–20 (2012).
- 368 22. Strbenac, D., Armstrong, N. J. & Yang, J. Y. H. Detection and classification of peaks in 5'
369 cap RNA sequencing data. *BMC Genomics* **14 Suppl 5**, S9 (2013).
- 370 23. Zhang, Y. *et al.* Model-based Analysis of ChIP-Seq (MACS). *Genome Biol.* **9**, R137
371 (2008).
- 372 24. Kharchenko, P. V, Tolstorukov, M. Y. & Park, P. J. Design and analysis of ChIP-seq
373 experiments for DNA-binding proteins. *Nat. Biotechnol.* **26**, 1351–1359 (2008).
- 374 25. Li, H. *et al.* The Sequence Alignment/Map format and SAMtools. *Bioinformatics* **25**,
375 2078–2079 (2009).
- 376 26. Lai, D., Proctor, J. R. & Meyer, I. M. On the importance of cotranscriptional RNA
377 structure formation. *RNA* **19**, 1461–1473 (2013).
- 378 27. Ringnér, M. & Krogh, M. Folding free energies of 5'-UTRs impact post-transcriptional
379 regulation on a genomic scale in yeast. *PLoS Comput. Biol.* **1**, e72 (2005).
- 380 28. Rabani, M. *et al.* Metabolic labeling of RNA uncovers principles of RNA production and
381 degradation dynamics in mammalian cells. *Nat. Biotechnol.* **29**, 436–42 (2011).
- 382 29. Yang, E. *et al.* Decay rates of human mRNAs: correlation with functional characteristics
383 and sequence attributes. *Genome Res.* **13**, 1863–72 (2003).
- 384 30. Tani, H. *et al.* Genome-wide determination of RNA stability reveals hundreds of short-
385 lived noncoding transcripts in mammals. *Genome Res.* **22**, 947–56 (2012).
- 386 31. Poptsova, M. S. *et al.* Non-random DNA fragmentation in next-generation sequencing. *Sci.*
387 *Rep.* **4**, 4532 (2014).
- 388 32. Lazarovici, A. *et al.* Probing DNA shape and methylation state on a genomic scale with

- 389 DNase I. *Proc. Natl. Acad. Sci. U. S. A.* **110**, 6376–81 (2013).
- 390 33. Papoulis, A. & Athanasios. Probability, random variables and stochastic processes. *New*
391 *York McGraw-Hill, 1984, 2nd ed.* (1984).
- 392 34. Hilbe, J. M. *Negative Binomial Regression.* (Cambridge University Press, 2011).
393 doi:10.1017/CBO9780511973420
- 394 35. Cameron, A. C. A. & Trivedi, P. K. *Regression Analysis of Count Data.* (Cambridge
395 University Press, 2013). doi:10.1017/CBO9781139013567
- 396 36. Hilbe, J. M. *Modeling Count Data.* (Cambridge University Press, 2014).
397 doi:10.1017/CBO9781139236065
- 398 37. Benjamini, Y. & Hochberg, Y. Controlling the False Discovery Rate: A Practical and
399 Powerful Approach to Multiple Testing. *J. R. Stat. Soc. Ser. B* **57**, 289–300 (1995).
- 400 38. Derrien, T. *et al.* Fast Computation and Applications of Genome Mappability. *PLoS One* **7**,
401 e30377 (2012).
- 402 39. Kawaji, H., Kasukawa, T., Forrest, A. & Carninci, P. The FANTOM 5 collection, a data
403 series underpinning mammalian transcriptome atlases in diverse cell types. *Sci. Data*
404 2016–2018 (2017). doi:10.1038/sdata.2017.113
- 405 40. Inoue, F. *et al.* A systematic comparison reveals substantial differences in chromosomal
406 versus episomal encoding of enhancer activity. *Genome Res.* **27**, 38–52 (2017).
407
408

409 **Supplementary Methods**

410 *Cell culture*

411 We cultured K562 cells (ATCC) in IMDM (Gibco #12440) supplemented with 10% fetal bovine
412 serum (FBS) and 1% pen/strep and maintained in a humidified chamber at 37°C with 5% CO₂.

413 We cultured HepG2 cells (ATCC) in EMEM (ATCC #30-2003) supplemented with 10% FBS
414 and 1% pen/strep, maintained in a humidified chamber at 37°C with 5% CO₂.

415

416 *Generating an ORI-STARR-seq input plasmid library*

417 We sonicated human male genomic DNA (Promega #G1471) using a Covaris S220 sonicator
418 (duty factor – 5%; cycle per burst – 200; 40 sec) and ran it on a 0.8% agarose gel to size-select
419 500 bp fragments. After gel purification using a MinElute Gel Extraction kit (Qiagen), we end-
420 repaired, ligated custom adaptors, and PCR-amplified DNA fragments using Q5 Hot Start High-
421 Fidelity DNA polymerase (NEB) (98°C for 30 sec; 10 cycles of 98°C for 10 sec, 65°C for 30 sec,
422 and 72°C for 30 sec; 72°C for 2 min) to add homology arms for Gibson assembly cloning.

423 We used AgeI-HF (NEB) and Sall-HF (NEB) to linearize the hSTARR-seq_ORI plasmid (gift
424 from Alexander Stark; Addgene plasmid #99296) and cloned the PCR products into the vector
425 using Gibson Assembly Master Mix (NEB); we set up 60 replicate reactions to maintain
426 complexity. We purified the assembly reactions using SPRI beads (Beckman Coulter), dialyzed
427 them using Slide-A-Lyzer MINI dialysis devices (ThermoScientific), and concentrated them
428 using an Amicon Ultra-0.5 device (Amicon). We transformed the reaction into MegaX
429 DH10BTM T1 electrocompetent cells (Thermo Fisher Scientific) (with 25 replicate
430 transformations to maintain complexity) and let them grow in 12.5L LB-Amp medium until they
431 reached an optical density of ~1.0. We extracted the plasmids using a Plasmid Gigaprep Kit

432 (Qiagen) and dialyzed the plasmid prep using Slide-A-Lyzer MINI dialysis devices before
433 electroporation.

434

435 *Electroporation-mediated transfection of ORI-STARR-seq input plasmid library into K562 and*
436 *HepG2 cell lines*

437 We electroporated the ORI-STARR-seq library using an AgilePulse Max (Harvard Apparatus)
438 and generated two biological replicate for each cell line. For K562 cells, we electroporated 5.6
439 mg of input plasmid library into 700 million cells per biological replicate by delivering three 500
440 V pulses (1 ms duration with a 20 ms interval). For HepG2 cells, we electroporated 8 mg of input
441 plasmid library into one billion cells in one replicate, and 5.6 mg into 700 million cells in another
442 replicate by delivering three 300 V pulses (5 ms duration with a 20 ms interval).

443

444 *Generation of an Illumina sequencing library*

445 *Output RNA library:* We harvested cells 24 hr after electroporation, and extracted total RNA
446 using an RNeasy Maxi kit (Qiagen). We further isolated polyA-plus mRNA using Dynabeads®
447 Oligo (dT) kit (ThermoFisher Scientific), treated it with TURBO DNase (Invitrogen), and
448 purified the reaction using an RNeasy MinElute Kit (Qiagen). We synthesized cDNA using
449 SuperScript III (ThermoFisher Scientific) with a custom primer that specifically recognizes
450 mRNAs that had been transcribed from the ORI-STARR-seq library. After reverse transcription,
451 we treated the reactions with a cocktail of RNase A and RNase T1 (ThermoFisher Scientific).
452 We split cDNA samples into 160 replicate sub-reactions, and PCR-amplified each sub-reaction
453 with a primer with a unique index (helping to identify PCR duplicates) using Q5 Hot Start High-
454 Fidelity DNA polymerase (NEB) with the following program: 98°C for 30 s; cycles of 98°C for

455 10 s, 65°C for 30 s, 72°C for 30 s (until they reached mid-log amplification phase; we cycled 18
456 cycles for K562 Rep.1; 16 cycles for K562 Rep. 2; 18 cycles for HepG2 Rep. 1; and 15 cycles
457 for HepG2 Rep2); 72°C for 2 min). After PCR, we re-combined all sub-reactions into one and
458 purified it with Agencourt Beads. We generated 100 bp paired-end reads for each biological
459 replicate on an Illumina Hiseq4000 at the University of Chicago Genome Facility.

460 *Input DNA library:* We PCR-amplified a total of 200 ng of input plasmid library (in 16 replicate
461 reactions) using Q5 Hot Start High-Fidelity DNA polymerase (NEB) with the following
462 program: 98°C for 30 s; 4 cycles of 98°C for 10 s, 65°C for 30 s, and 72°C for 20 s; 8 cycles of
463 98°C for 10 s and 72°C for 50 s; 72°C for 2 min). After PCR, we combined all products into one
464 and purified it with Agencourt Beads. We generated 100 bp paired-end reads on an Illumina
465 Hiseq4000 at the University of Chicago Genome Facility.

466

467 *Sequencing and preprocessing*

468 For each of 160 replicates, paired-end sequencing reads were aligned to the human reference
469 genome hg38 using BWA-mem (v0.7.17). Alignments were filtered against unmapped,
470 secondary alignments, mapping quality score less than 30, and PCR duplicates using SAMtools
471 (v1.5) and Picard (v2.9.0). All of replicates were pooled and sorted for downstream analysis.

472

473 *Negative binomial distribution*

474 A negative binomial distribution, which arises from Gamma-Poisson mixture, can be
475 parametrized for $y \geq 0$ as follows.

476

$$Pr(Y = y_i | \mu_i, \theta) = f_Y(y_i; \mu_i, \theta) = \frac{\Gamma(y_i + \theta)}{\Gamma(y_i + 1) \cdot \Gamma(\theta)} \cdot \left(\frac{\theta}{\theta + \mu_i}\right)^\theta \cdot \left(\frac{\mu_i}{\theta + \mu_i}\right)^{y_i}$$

477

478 Rearranging gives:

479

$$f_Y(y_i; \mu_i, \theta) = \frac{\Gamma(y_i + \theta)}{\Gamma(y_i + 1) \cdot \Gamma(\theta)} \cdot \left(\frac{1}{1 + \frac{\mu_i}{\theta}} \right)^\theta \cdot \left(\frac{\frac{\mu_i}{\theta}}{1 + \frac{\mu_i}{\theta}} \right)^{y_i}$$

$$f_Y(y_i; \theta, \mu_i) = \frac{\Gamma(y_i + \theta)}{\Gamma(y_i + 1) \cdot \Gamma(\theta)} \cdot \left(\frac{\mu_i}{\theta} \right)^{y_i} \left(\frac{1}{1 + \frac{\mu_i}{\theta}} \right)^{\theta + y_i}$$

$$f_Y(y_i; \theta, \mu_i) = \frac{\Gamma(y_i + \theta)}{\Gamma(y_i + 1) \cdot \Gamma(\theta)} \cdot \left(\frac{\mu_i}{\theta} \right)^{y_i} \left(\frac{\theta}{\theta + \mu_i} \right)^{\theta + y_i}$$

$$f_Y(y_i; \theta, \mu_i) = \frac{\Gamma(y_i + \theta)}{\Gamma(y_i + 1) \cdot \Gamma(\theta)} \cdot \frac{\mu_i^{y_i} \theta^\theta}{(\theta + \mu_i)^{\theta + y_i}}$$

480

481 *Alternative parametrization of negative binomial regression using a rate model*

482 Alternative parametrization allows STARR-seq data to be modelled as a rate model. In contrast

483 to using input coverage as one of the covariates, we can consider it as “exposure” to output

484 coverage. This “trick” allows us to directly model the basal transcription rate (the ratio of RNA

485 to DNA) as a rate response variable. We defined the transcription rate (RNA to DNA ratio) as a

486 new variable, π_i .

487

$$\frac{y_i}{t_i} = \pi_i$$

488

489 If we assume the majority of genomic bins will have the basal transcription rate, we can model
490 the transcription rate at each i -th bin following the traditional negative binomial (NB2)
491 distribution.

492

$$\pi_i \sim NB\left(\frac{\mu_i}{t_i}, \theta\right)$$

493

494 The expected basal transcription, $E(\pi_i)$, becomes the mean incidence rate of y_i per unit of
495 exposure, t_i .

496

$$E\left(\frac{y_i}{t_i}\right) = \frac{\mu_i}{t_i}$$

497

498 By normalizing μ_i by t_i , we are modeling a rate instead of a discrete count using the negative
499 binomial distribution. The regression term for the expected transcription rate can be expressed in
500 terms of a linear combination of explanatory variables, j covariates (\vec{x}).

501

$$\ln \frac{\mu_i}{t_i} = \beta_1 x_{i1} + \beta_2 x_{i2} + \dots + \beta_j x_{ij}$$

502

503 Rearranging in terms of the expected value of y , or μ , gives

504

$$\begin{aligned}\ln \mu_i - \ln t_i &= \beta_1 x_{i1} + \beta_2 x_{i2} + \dots + \beta_j x_{ij} \\ \ln \mu_i &= \ln t_i + \beta_1 x_{i1} + \beta_2 x_{i2} + \dots + \beta_j x_{ij} \\ \mu_i &= \exp(\ln t_i + \beta_1 x_{i1} + \beta_2 x_{i2} + \dots + \beta_j x_{ij})\end{aligned}$$

505

506 The natural log of t_i on the RHS ensures μ_i is normalized in the model, acting as an offset
507 variable. In STARRPeaker software, we allow users to optionally choose this alternative rate
508 model (implemented as “mode 2”) instead of the default covariate model described in the main
509 text.

510

511 *BasicSTARRseq*

512 We used BasicSTARRseq R package version 1.10.0 downloaded from Bioconductor
513 (<https://bioconductor.org/packages/release/bioc/html/BasicSTARRseq.html>). We used default
514 setting as described in the software manual (minQuantile = 0.9, peakWidth = 500, maxPval =
515 0.001, deduplicate = TRUE, model = 1) to call peaks.

516

517 *MACS2*

518 We used MACS2 version 2.1.1²³ at the recommended default setting, except for allowing
519 duplicates in read (--keep-dup all), since our STARR-seq dataset was multiplexed. We called
520 peaks with an FDR cutoff of 0.01, as recommended by the author of the software.

521

522 **Supplementary Tables**

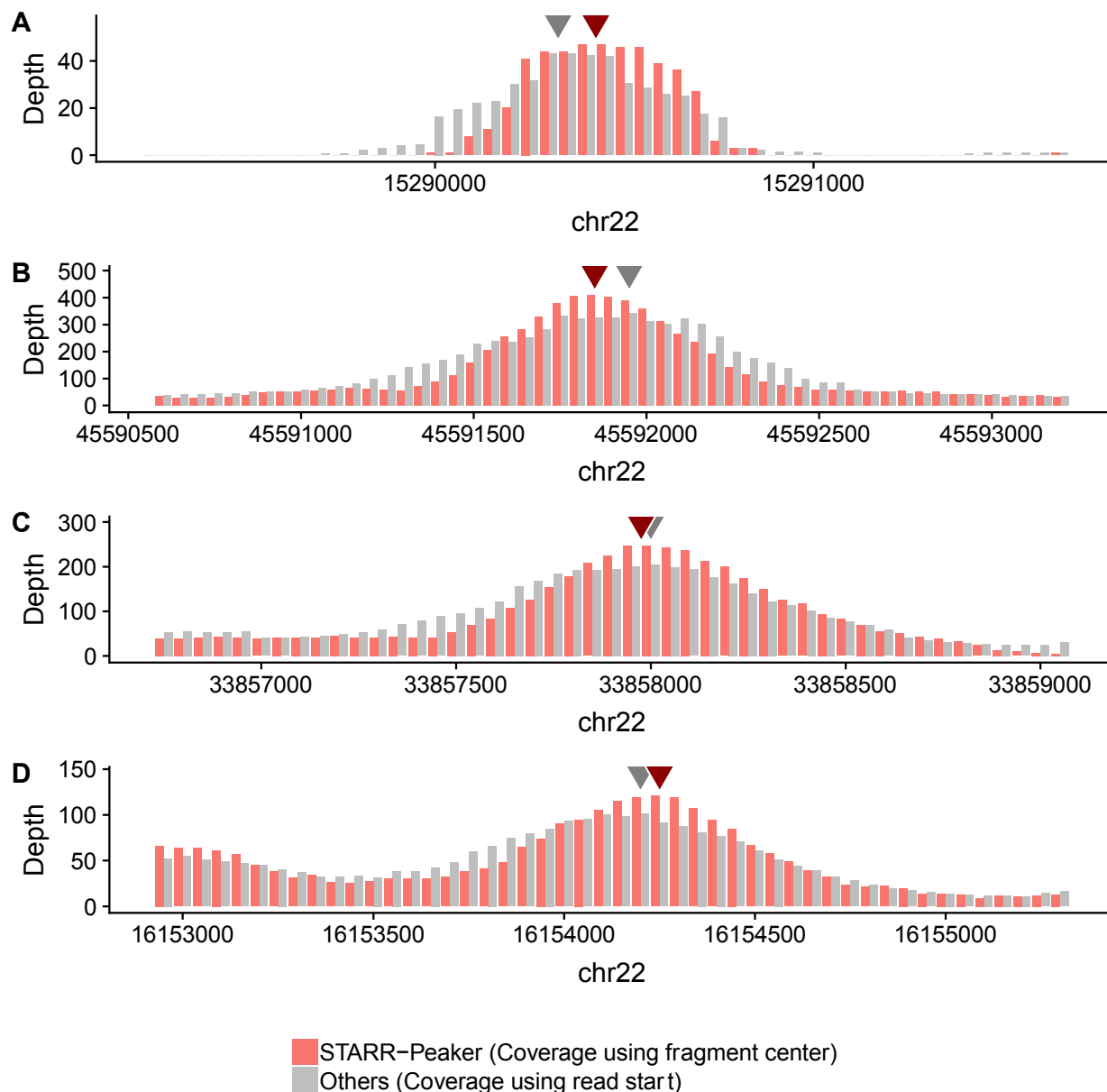
523 Table S1 contains significant peaks called by STARRPeaker.

524 Table S2 contains various statistics from comparing STARRPeaker peaks to peaks called by
525 BasicSTARRseq and MACS2.

526 Table S3 contains list of data sources and accession number used for the analysis.

527

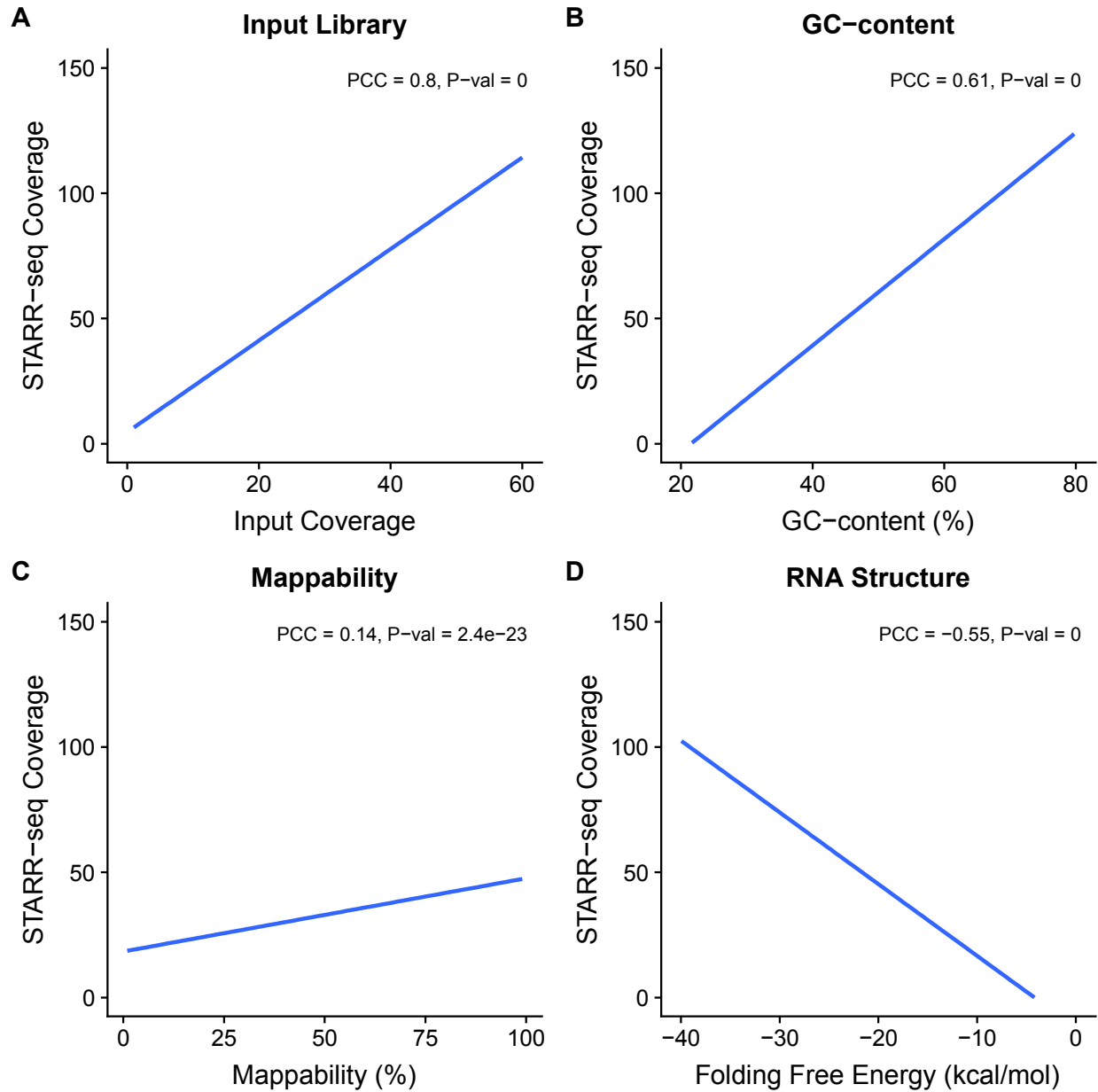
528 **Figures**



529

530 **Figure 1** Comparison of STARR-seq coverage calculated using fragment center to
531 using read start position. (A)-(D) shows examples drawn from K562 STARR-seq data.
532 Triangle indicates the summit of coverage. Read depth was normalized, since 2 paired
533 reads correspond to 1 fragment.

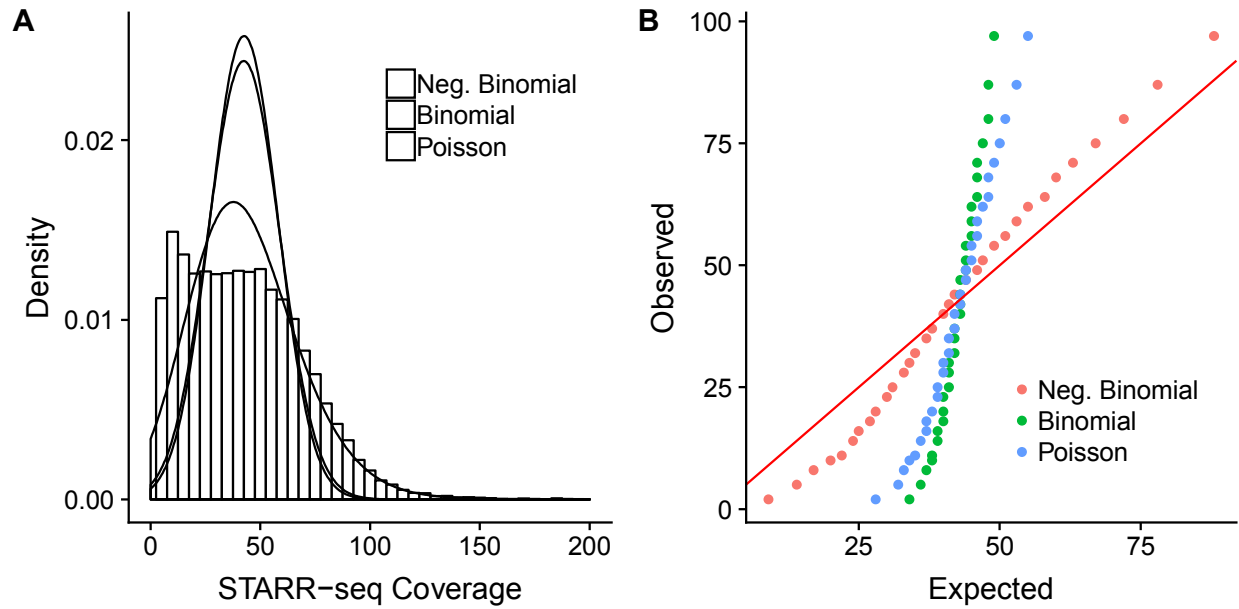
534



535

536 **Figure 2** Confounding factors in the STARR-seq assay. STARR-seq output and input
537 coverages are significantly correlated with (A) input coverage (B) GC-content (C)
538 mappability, and (D) RNA structure folding. PCC: Pearson Correlation Coefficient. Plots
539 were from a sampling of 5,000 random genomic bins.

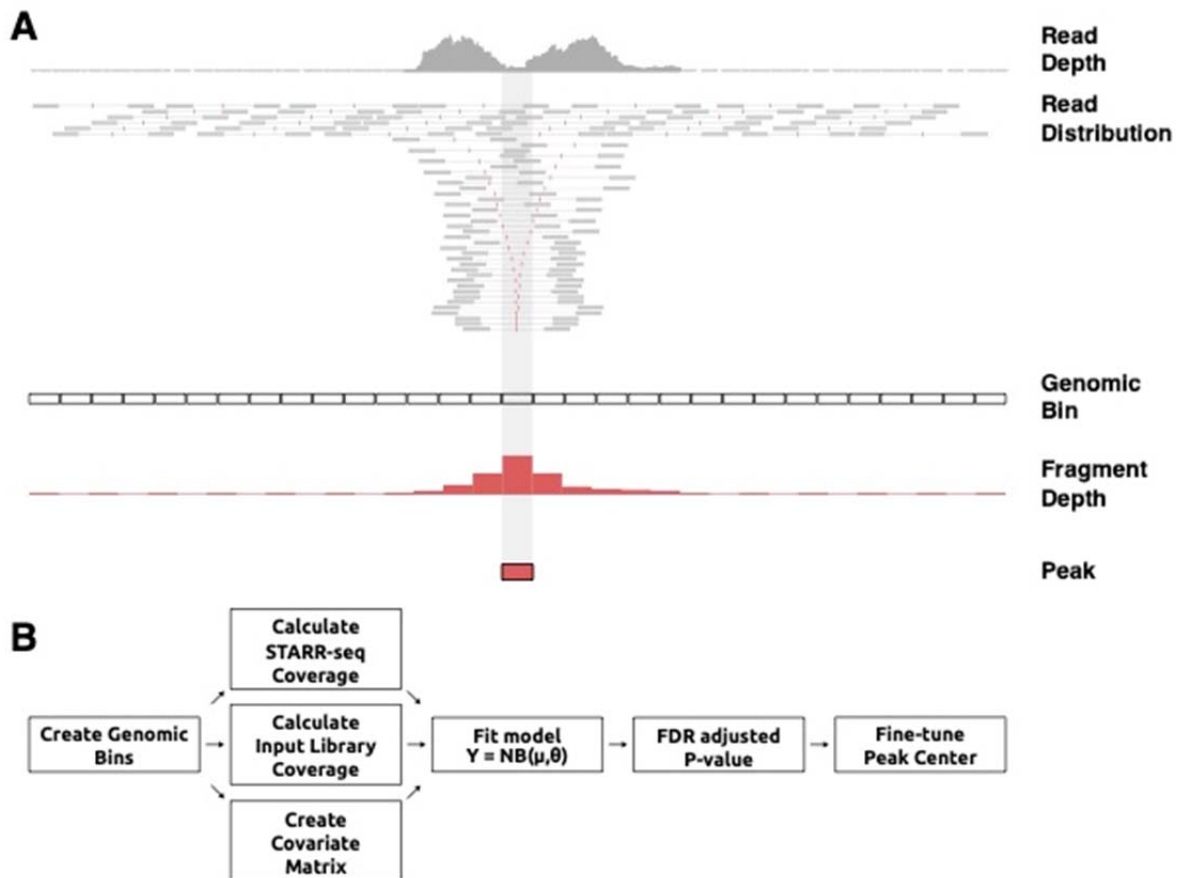
540



541

542 **Figure 3** STARR-seq coverage is fitted against simulated coverage using three
543 distribution models; negative binomial, binomial, and Poisson. (A) Density histogram of
544 simulated distribution against STARR-seq coverage. (B) Q-Q plot of simulated
545 distribution against STARR-seq coverage. The red solid line represents where the
546 observed count equals the expected count.

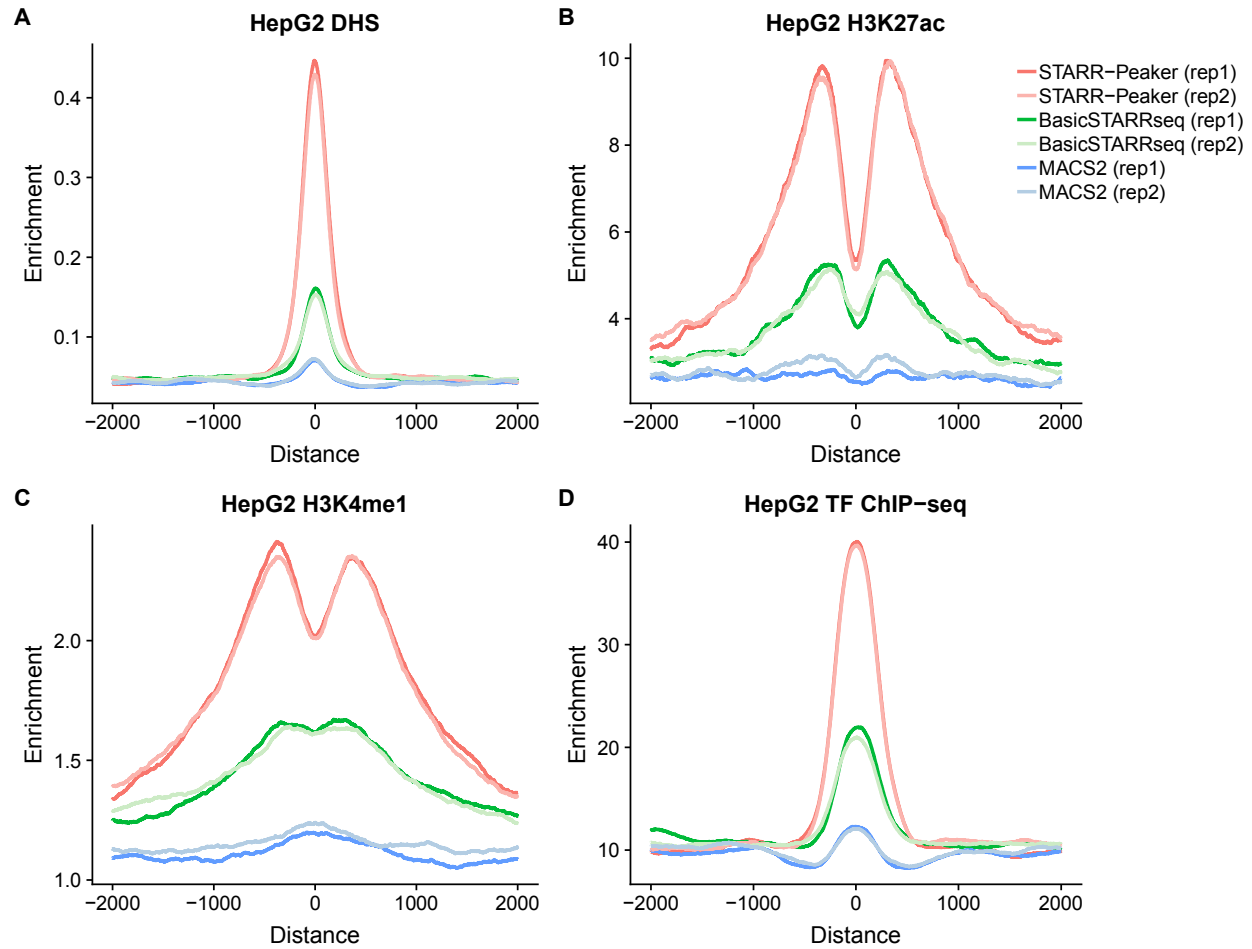
547



548

549 **Figure 4** Overview of STARRPeaker peak-calling scheme. (A) In contrast to using read depth
550 (grey), fragment depth (red) offers more precise and sharper STARR-seq coverage. Fragment
551 inserts are directly inferred from properly paired-reads. (B) Workflow of STARRPeaker
552 describing how coverage is calculated for each genomic bin and modelled using negative
553 binomial regression model. The analysis pipeline can largely be divided into four steps: (1)
554 Binning the genome (2) Calculating coverage and computing covariate matrix (3) Fitting the
555 STARR-seq data to the NB regression model (4) Peak calling, multiple hypothesis testing
556 correction, and adjustment of the center of peaks

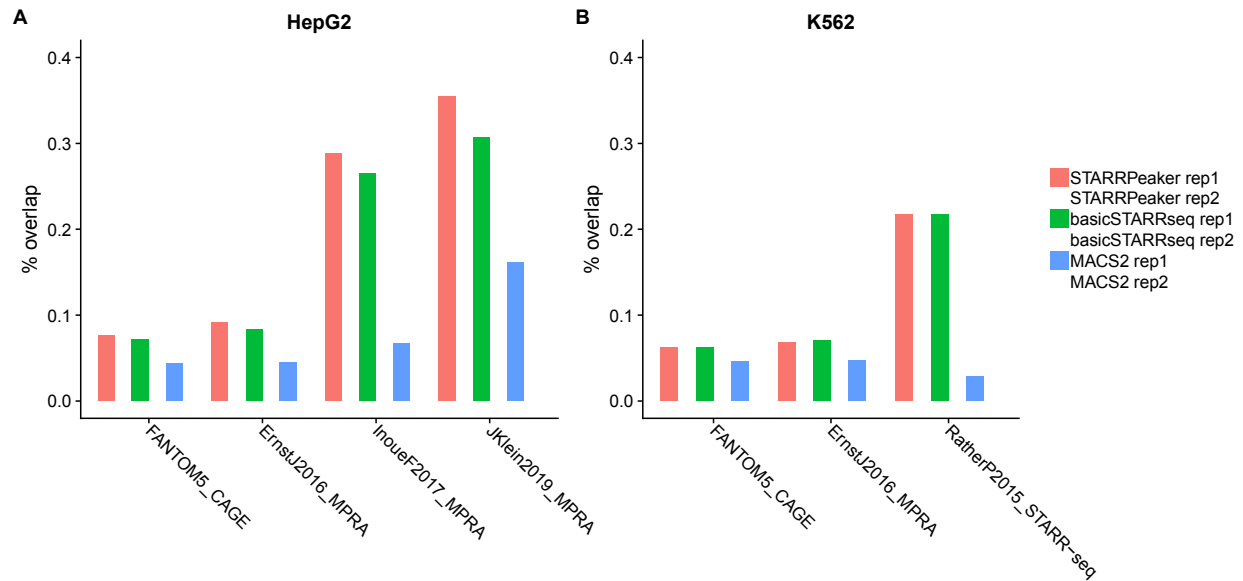
557



558

559 *Figure 5* Enrichment of epigenetic signals around peaks. All peaks were centered at the summit,
560 uniformly thresholded using P -value < 0.001 , and 10,000 peaks were randomly selected.
561 Aggregated read depth at 2000 bp upstream and downstream were plotted for (A) DNase-seq (B)
562 H3K27ac (C) H3K4me1 (D) Aggregated TF ChIP-seq profile. For TF ChIP-seq, high
563 enrichment indicates TF binding hotspots

564



565

566 **Figure 6** Comparison of peaks using external dataset. Peaks identified from STARRPeaker as
567 well as BasicSTARRseq and MACS2 were compared against published dataset. For a fair
568 comparison, 100,000 peaks were randomly drawn from peaks identified by each peak caller
569 using the recommended settings, and the fraction of overlap was computed for each replicate.
570 We considered it as an overlap when at least 50% of peaks intersected each other.